Available online at www.sciencedirect.com
ScienceDirect
Catalysis Today 133–135 (2008) 168–173
CATALYSIS TODAY
www.elsevier.com/locate/cattod

Surface reactivity of zinc-modified hydroxyapatite

Rafaella M.B. Faria, Deborah V. César, Vera M.M. Salim *

NUCAT, Programa de Engenharia Química, COPPE, Universidade Federal do Rio de Janeiro, Cidade Universitária, Centro de Tecnologia, Bloco G/115, CEP 21945-970, Rio de Janeiro, RJ, Brazil

Available online 12 February 2008

Abstract

Surface reactivity of hydroxyapatite (Hap), $Ca_{10}(PO_4)_6(OH)_2$, and zinc-Hap was evaluated using temperature-programmed desorption (TPD) of ethanol and diffuse reflectance infrared spectroscopy (DRIFTS). Hap was prepared by the precipitation method and the Zn-based catalysts were prepared by the ionic exchange method ($ZnHap_{troc}$) and by zinc oxide deposition ($ZnHap_{dep}$). X-ray diffraction (XRD) results have shown the Ca^{2+} substitution by Zn^{2+} ions for the catalyst prepared by ionic exchange method and a zinc oxide formation as a segregated phase after zinc deposition. TPD-ethanol analyses showed that Hap has catalytic activity to ethanol decomposition and low surface acidity. DRIFTS results showed ethoxide species formation at the surface of $ZnHap_{troc}$, which undergoes transformation into acetate and carbonate species with increasing temperature. The catalyst prepared through the ionic exchange method ($ZnHap_{troc}$) showed high selectivity to the ethanol dehydrogenation reaction.

Keywords: Zinc; Hydroxyapatite; TPD-ethanol; DRIFTS

1. Introduction

Synthetic hydroxyapatites (Hap), $Ca_{10-z}(HPO_4)_z(PO_4)_{6-z}(OH)_{2-z}$ $[0 < z < 1]$, are widely used as bioceramic materials and as adsorbent for separation of biomolecules. Recently, these materials have been used as adsorbents for heavy metals [1], as support [2,3] and as catalysts in oxidation [4,5], dehydrogenation [6], dehydration [7], acid–basic [8], and partial oxidation reactions [9]. Their catalytic performance depends on the lattice substitutions and on the stoichiometry, which can vary with Ca/P molar ratios from 1.5 to 1.67. Stoichiometric apatite ($z = 1$) presents basic properties while the non-stoichiometric one exhibit acidic sites [10]. Two unconnected channels form the lattice of stoichiometric calcium hydroxyapatite [11]: the first has a diameter of 2.5 Å and is surrounded by Ca^{2+} ions (denoted Ca (I)). The second type plays an important role in the apatites properties. It has a diameter of around 3.5 Å and is also surrounded by oxygen and Ca^{2+} ions in a coordination of 7 (denoted Ca(II)). These channels host OH groups along the *c* axis to balance the positive charge of the matrix. The environment around the OH^- sites is very favorable for substitutions because it allows one to control the acid site strength and also the ratio between Lewis and Brönsted acid sites. The apatite structure possesses a great flexibility in accepting substitutions in its lattice and substitutions of the calcium ions (Ca^{2+}/M^{2+}) [12]. The ions calcium substitution allows the introduction of an active metal into the lattice becoming a potentially interesting material as catalyst for reactions such as methane activation [9] and oxidative dehydrogenation. According to the literatures, the incorporation of a transition metal, such as Ni^{2+}, Cu^{2+} and Co^{2+} into the lattice creates new redox sites that favor the activity of dehydrogenation reactions [5,13]. Therefore, the possibility of controlling the stoichiometry and precise ion substitutions make hydroxyapatite a very attractive material for structure–property investigations, mainly for the development of catalysts with specific properties.

In previous studies we have demonstrated that anions substitutions and thermal treatment caused changes in the acid strength distribution and increased the overall acidity and acid site density ($\mu mol/m^2$) of the Hap [14,15]. In more recent works, the use of Hap as support and the influence of its acid/basic properties on the activity and selectivity in ethanol partial oxidation have been evaluated for catalysts containing Zn, Co, Fe or Cu supported on Hap. The catalysts had been prepared by two methods: ionic exchange and oxide deposition. In both

* Corresponding author.
E-mail address: vera@peq.coppe.ufrj.br (V.M.M. Salim).

0920-5861/$ – see front matter
doi:10.1016/j.cattod.2007.12.114

methods the ZnHap catalysts presented high selectivity for H_2 production [16].

This work investigates the effect of the preparation method on the surface properties of Hap and Zn-Hap catalysts. Ethanol reactivity was evaluated using temperature-programmed desorption (TPD-ethanol) and *in situ* diffuse reflectance infrared spectroscopy (DRIFTS).

2. Experimental

2.1. Hydroxyapatite preparation

$Ca_{10}(PO_4)_6(OH)_2$ was prepared by the precipitation method from calcium nitrate solutions 0.50 M (Vetec 99%): solution A, and phosphate of ammonium 0.30 M (Vetec 99%): solution B. The pH was adjusted at 10–11 by addition of NH_4OH (0.3 M). Solution B was added (rate of 4 mL/min) to solution A, kept under magnetic agitation at 80 °C (±5 °C). The mixture was then kept at 80 °C/2 h, filtered and washed with hot water (80 °C) until obtaining a filtered solution with pH of 7. The solid was dried for 24 h at 100 °C and then sieved at 150 and 300 mesh.

2.2. Catalysts preparation

- *Ionic exchange method*: A solution of $Zn(NO_3)_2{\cdot}H_2O$, 0.1 M was kept in contact with 10 g of Hap for 48 h under agitation at room temperature to obtain 10% of Zn. The solid was filtered, dried at 100 °C for 24 h and calcined at 350 °C for 3 h. For $ZnHap_{troc1}$ sample 100 mL of the solution was used, whereas for $ZnHap_{troc2}$ 200 mL of the zinc solution was used.
- *Deposition method*: A mixture of Hap and zinc nitrate solution with a suitable Zn loading to obtain 10% of ZnO was evaporated in a rotary vacuum at 100 °C. The material was dried at 100 °C for 24 h and then calcined at 350 °C for 3 h. Two samples were prepared: $ZnHap_{dep1}$, 15 mL of Zn solution (0.1 M):1 g Hap and $ZnHap_{dep2}$, 3 mL of Zn solution (0.4 M):1 g Hap, in order to evaluate the influence of the zinc solution volume/support weight ratio.

2.3. Characterization

The Ca/P ratio and the metal loading of the samples were determined by X-ray fluorescence (XRF), using a Rigaku Sequential Spectrometer (RIX 3100) equipment with a Rh source. The textural properties were determined by nitrogen adsorption at −196 °C (Micromeritics ASAP 2000). The samples were out gassed (5.10^{-3} Torr) at 150 °C for 12 h prior to N_2 adsorption. X-ray diffraction (XRD; Rigaku model Miniflex TG) was applied to analyze the different phases in the samples. The measurements were performed with scan speed of $0.05^\circ\ min^{-1}$ using Cu Kα radiation and $10^\circ < 2\theta < 80^\circ$. The identification of the phases was carried out using the standard database ICDD-PDF-09-0432.

Temperature-programmed desorption (TPD-ethanol): The apparatus used in this study was a unit equipped with an online quadrupole mass spectrometer (Balzers QMS 422). The samples were pretreated at 300 °C for 1 h in flowing He (30 mL/min) and cooled up to 25 °C. The ethanol was chemisorbed at room temperature by flowing (96.6 μmol) CH_3CH_2OH/He (60 mL/min) mixture for 30 min. Afterwards the samples were purged for 1 h in flowing He (60 mL/min) to remove any physically adsorbed ethanol and then the temperature was increased at a heating rate of 10 °C/min up to 700 °C. The desorbing species were monitored by their characteristic mass fragmentation patterns (*m/e*): 45, 31, *27* (ethanol); *2* (H_2); 28, 27, *26* (ethylene); 45, *31*, 29 (diethyl ether); 44, 43, *29* (acetaldehyde); *44*, 28 (CO_2); 29, *28* (CO); *45*, 43, 29 (acid acetic); *58*, 43, 15 (acetone); 17, 16, *15* (CH_4) and *18*, 17, 16 (H_2O). The dominant fragment of each desorbed product was quantitatively analyzed after discounting the ion/mass fragmentation interference.

Diffuse Reflectance Fourier Transform Infrared Spectroscopy (DRIFTS): The analyses were carried out in a Nicolet spectrometer (Nexus 470) equipped with an accessory of diffuse reflectance (Spectra-Tech) with a chamber for heating up to high temperatures, ZnSe windows, resolution of 4 cm^{-1} and MCT-A detector. The samples were treated *in situ* at 350 °C in flowing He for 1 h, followed by cooling until room temperature. Ethanol chemisorption was performed by exposing the catalyst to a flowing (18.2 μmol) CH_3CH_2OH/He (30 mL/min) mixture for 30 min. After removing the reversible adsorbed ethanol using flowing He (30 mL/min), the catalyst was heated at different temperatures (100, 200, 300, 400 and 500 °C) under flow of He, and a spectrum was registered. The spectrum of the treated sample was used as background.

3. Results and discussion

A series of Hap was prepared in order to evaluate the reproducibility of the preparation method of stoichiometric Haps' through the preparation of this material in triplicate.

Diffractogram analysis (Fig. 1) allowed the identification of a hexagonal phase with lattice parameters ($a = b = 0.9407$ nm, $c = 0.6873$ nm, $\alpha = \beta = 90^\circ$ and $\delta = 120^\circ$) that are characteristic of hydroxyapatite, which is in accordance with the database ICDD-PDF-09-0432. All diffractograms of Hap samples (not shown) were similar and presented the same lattice parameters values. The Ca/P ratio values, obtained by XRF analyses were between 1.64 and 1.67, which are characteristic of a stoichiometric Hap.

For samples containing zinc, Table 1 presents their Zn loading and Ca/P ratio. A decrease in the Ca/P ratio for the catalysts prepared by ionic exchange ($ZnHap_{troc1}$ and $ZnHap_{troc2}$) was observed, indicating the Ca^{2+} substitution by Zn^{2+} in the lattice of these samples. It was observed that Zn^{2+} cation incorporation was limited by a value of 6–7% of metal incorporated. Miyaji et al. [10] have estimated a limit of 15 mol% for Zn substitution in the Hap lattice, once the crystallinity of the hydroxyapatite decreases with increasing Zn fraction. In our case, it was verified (Table 1) that the Zn^{2+} cation incorporation by ionic exchange method was limited for a value of 6–7% of metal incorporated, and it was possibly caused by a diffusion limit.

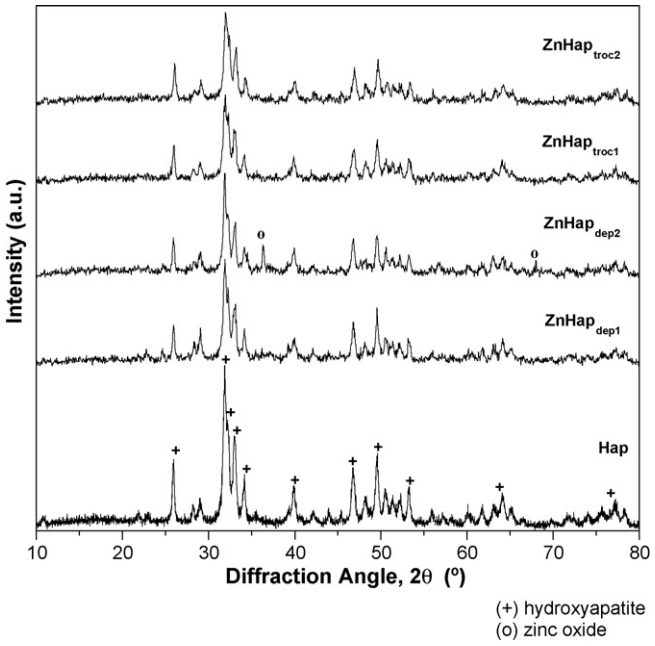

Fig. 1. Powder XDR patterns of the Hap, $ZnHap_{dep1}$, $ZnHap_{dep2}$, $ZnHap_{troc1}$ and $ZnHap_{troc2}$.

According to the textural analyses, $S_{BET} = 13\ m^2/g$, $V_p = 0.05\ cm^3/g$ and $d_p = 139$ Å was found for the catalysts prepared by the deposition method. For those prepared by ionic exchange, $S_{BET} = 22\ m^2/g$, $V_p = 0.13\ cm^3/g$ and $d_p = 240$ Å were obtained. It is worth noting that the evaporation method favored a decrease in the specific surface area.

X-ray diffraction results for $ZnHap_{dep1}$ sample (Fig. 1) presented only the characteristic peaks of Hap (+); the absence of ZnO phase could be due to the smaller crystallite size of this oxide. However, for $ZnHap_{dep2}$, prepared with lower volume of zinc solution, characteristic peaks of the Hap (+) and ZnO (o) were observed. These results show the influence of the zinc solution concentration on the preparation method, which favors the formation of segregated phases for high zinc concentrations. The crystalline structure of Hap did not change in both catalysts as demonstrated by their lattice parameters in Table 2. The catalysts prepared by ionic exchange method, presented only the characteristic peaks of Hap (+); a distortion in the crystalline structure of the original Hap after the substitution of Ca^{2+} for Zn^{2+} ions is corroborated by the lattice parameters variation (Table 2).

The surface reactivity of the $ZnHap_{troc2}$ and $ZnHap_{dep2}$ samples were evaluated, once they presented significant differences in relation to the phase formed, for $ZnHap_{dep2}$ sample the ZnO was as segregated phase while for the $ZnHap_{troc2}$ sample, the Zn was incorporated into the lattice.

Table 1
Zinc loading and Ca/P ratio

	$ZnHap_{dep1}$	$ZnHap_{dep2}$	$ZnHap_{troc1}$	$ZnHap_{troc2}$
% Zn	13.25	10.30	5.84	6.96
Ca/P ratio	1.70	1.69	1.57	1.56

Table 2
XRD results—identified phases and lattice parameters of Hap and catalysts

Sample	Phase	Lattice parameters			
		a (nm)	c (nm)	α (°)	γ (°)
Hap	Hap	0.9407	0.6873	90	120
$ZnHap_{dep1}$	Hap	0.9404	0.6878	90	120
$ZnHap_{dep2}$	Hap	0.9400	0.6878	90	120
	ZnO	0.3249	0.5204	90	120
$ZnHap_{troc1}$	Hap	0.9409	0.6871	90	120
$ZnHap_{troc2}$	Hap	0.9385	0.6898	90	120

The literatures has shown that the TPD technique can provide a better understanding of ethanol interactions with surface active sites of catalysts such as Rh–Pt/CeO_2 [17], Co/ZnO [18], Ni/Al_2O_3, Ni/La_2O_3 and Ni/(La_2O_3/Al_2O_3) [19]. It was verified that supported catalyst such as Al_2O_3 and La_2O_3 strongly interact with ethanol at relatively low temperatures. Also, Al_2O_3 promotes dehydration and cracking while La_2O_3 primarily promotes dehydrogenation and cracking [19].

TPD profiles after ethanol adsorption on Hap (Fig. 2) show that the Hap surface presents reactivity with desorption of different products. There are two main temperature domains, between 50–350 and 350–800 °C. In the former, we observed molecular ethanol desorption ($m/e = 27$), H_2 ($m/e = 2$), ethylene ($m/e = 26$), diethyl ether ($m/e = 31$), acetaldehyde ($m/e = 29$), CO_2 ($m/e = 44$), CO ($m/e = 28$) and methane ($m/e = 15$), suggesting that these are produced from the decomposition of the same intermediate species adsorbed on the hydroxyapatite surface. At temperatures between 350 and 800 °C, H_2 ($m/e = 2$), CO_2 ($m/e = 44$), CO ($m/e = 28$) and ethylene ($m/e = 26$) were observed. The mass fragmentation

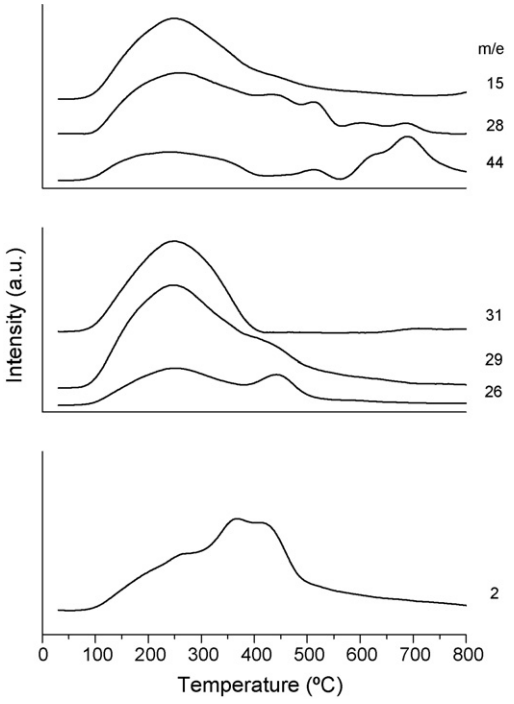

Fig. 2. Product desorption profiles from TPD-ethanol on Hap.

Table 3
Products of the TPD-ethanol on Hap and catalysts

Product	Yield ($\mu mol/g_{sample}$)		
	Hap	$ZnHap_{dep2}$	$ZnHap_{troc2}$
Ethanol	39.9	24.2	39.5
H_2	17.5	12.4	78.3
Ethylene	23.1	19.2	20.1
Acetaldehyde	87.1	104.9	110.4
Diethyl ether	17.8	38.2	16.8
CO_2	19.1	26.8	47.1
CO	76.7	74.6	65.9
CH_4	29.2	62.2	33.3

patterns $m/e = 45$ (acid acetic) and 58 (acetone) were not detected.

Table 3 shows the quantification results and we observed that, for Hap, acetaldehyde was the major product formed (87.1 $\mu mol/g_{sample}$), suggesting that ethanol dehydrogenation reaction occurs mainly in the 50–500 °C temperature range. The small amount of ethylene (23.1 $\mu mol/g_{sample}$) demonstrates the low acidity of the Hap.

For $ZnHap_{dep2}$ (Fig. 3) the temperature of desorption was observed only in the range of 50–300 °C where ethylene ($m/e = 26$), diethyl ether ($m/e = 31$), acetaldehyde ($m/e = 29$), CO_2 ($m/e = 44$), CO ($m/e = 28$), H_2 ($m/e = 2$) and methane ($m/e = 15$) desorption occurred. The increase in acetaldehyde formation (104.9 $\mu mol/g_{sample}$, Table 3), in comparison to Hap, suggests that the zinc addition favored the dehydrogenation reaction. Moreover, a reduction in the amount of ethylene (19.2 $\mu mol/g_{sample}$) was observed indicating a decrease in the Hap acidity after Zn deposition. The low H_2 formation (12.4 $\mu mol/g_{sample}$) could be attributed to the high CH_4 (62.2 $\mu mol/g_{sample}$) and CO (74.6 $\mu mol/g_{sample}$) due to the decomposition reaction of the ethoxide species adsorbed [12]: $CH_3CH_2O–M^{n+} \rightarrow CH_4 + CO + 1/2H_2 + M^{n+}$.

Desorption profiles for $ZnHap_{troc2}$ (Fig. 4) showed a different behavior when compared with that of $ZnHap_{dep2}$. Two main temperature domains were verified, first between 50 and 350 °C and another one at 350–700 °C. The desorption of molecular ethanol ($m/e = 27$, not shown) and diethyl ether ($m/e = 31$) occurred between 50 and 200 °C; while ethylene ($m/e = 26$), acetaldehyde ($m/e = 29$) and methane ($m/e = 15$) desorbed up to 350 °C. The CO_2 ($m/e = 44$) and CO ($m/e = 28$) desorption were verified at high temperatures. The H_2 formation ($m/e = 2$; 78.3 $\mu mol/g_{sample}$) presented a maximum at 280 °C and is significantly higher than for the other studied samples (Table 3); acetaldehyde formation also increased (110.4 $\mu mol/g_{sample}$). The lower ethylene and diethyl ether formation (products of dehydration) is an indicative of less acidity for the $ZnHap_{troc2}$ sample.

In order to evaluate the intermediate species formed on the surface of the $ZnHap_{troc2}$ catalyst after ethanol adsorption, which produced the highest H_2desorption, DRIFTS analysis was carried out (Fig. 5).

Ethanol adsorption at room temperature produced bands at 2974, 2933, 2874, 1660, 1480, 1427, 1391, 1302 and 1134 cm^{-1}. The bands at 2974, 2933, 2874 (ν CH_3, CH_2), 1480 (δ_{as} CH_3, CH_2), 1391 (δ_s CH_3, CH_2) are attributed to surface ethoxide species [20,21]. In accordance with the literature, primary alcohols adsorb on the metallic oxide surfaces as alkoxide from the scission of the O–H bond [20].

The bands at 1302 cm^{-1} (δ_s CH_3) and at 1427 cm^{-1} (ν_s OCO) suggested formation of acetate species adsorbed on zinc [22], whereas the bands at 1660 and 1134 cm^{-1} can be related

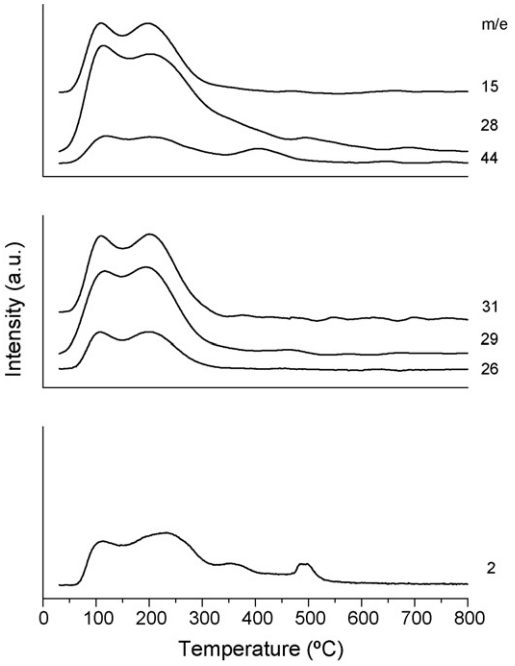

Fig. 3. Product desorption profiles from TPD-ethanol on $ZnHap_{dep2}$.

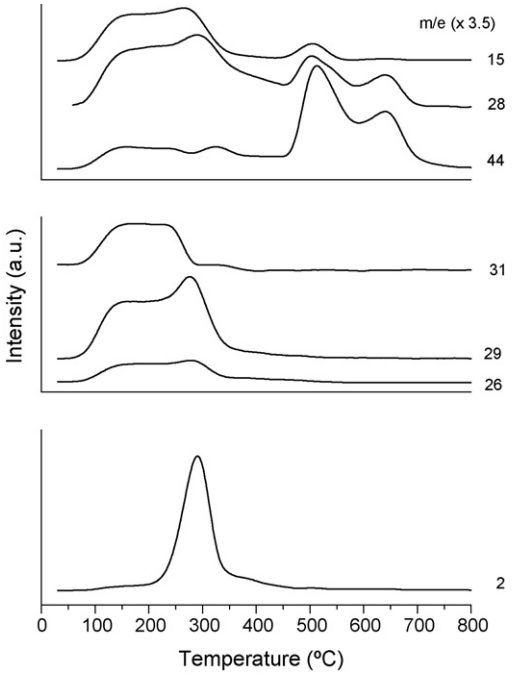

Fig. 4. Product desorption profiles from TPD-ethanol on $ZnHap_{troc2}$.

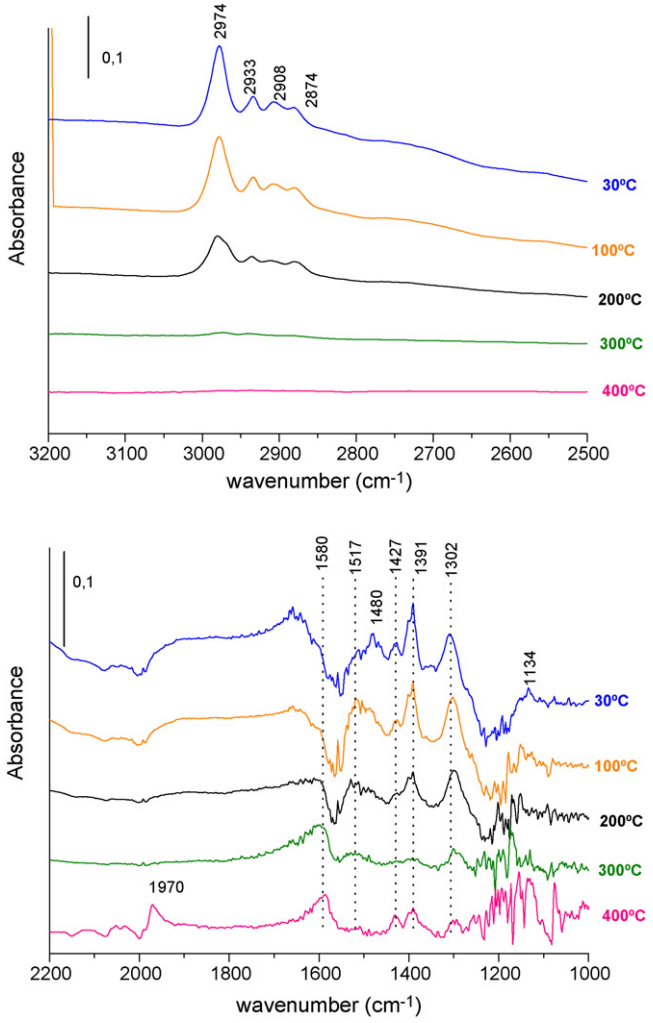

Fig. 5. DRIFT spectra after ethanol at 400 °C on $ZnHap_{troc2}$ catalysts.

to undissociated ethanol. Heating to 100 °C produces a slightly change in the DRIFT spectra, a reduction of the band intensity of ethoxide species (1480 and 1391 cm^{-1}) and a slight increase of acetate species (1302 cm^{-1}) with formation of a band around 1517 cm^{-1}. The formation of acetate adsorbed on bulk zinc oxide was observed by Yee et al. [23] at 1550 cm^{-1} and attributed to the vibration mode ν_{as} OCO. In the present work, we did not observe the ZnO formation as a segregated phase for this sample. Therefore, the band at 1517 cm^{-1} could be assigned to the adsorption of acetate species on Zn^{2+} onto the Hap lattice. Further heating to 200 °C showed that undissociated ethanol was completely desorbed. Moreover, a decrease in the band intensity due to ethoxide (3000–2700, 1480 and 1391 cm^{-1}) and to acetate (1302, 1427, 1517 cm^{-1}) was observed at this temperature. After heating at 300 °C, the bands assigned to ethoxide species were not observed, exhibiting only those related to acetates adsorbed on zinc (1302 and 1517 cm^{-1}), though with lower intensity. A new band at 1580 cm^{-1} was observed and it can be assigned to the formation of carbonate–carboxylate and acetate species. The accurate identification of these bands is difficult, since those bands of carbonate–carboxylate can be observed in the region between 1000 and 1700 16 cm^{-1} [22]:

(i) *Carboxylate*: 1560–1630 cm^{-1} (ν_{as} COO^-) and 1350–1420 cm^{-1} (ν_s COO^-) and absence of bands in the region of 1000 cm^{-1}.
(ii) *Monodentade carbonate*: 1530–1470 cm^{-1} (ν_{as} COO^-) and 1300–1370 cm^{-1} (ν_s COO^-), 1080–1040 (ν C–O).
(iii) *Bidentade carbonate*: 1530–1620 cm^{-1} (ν C–O), 1270–1250 cm^{-1} (ν_{as} COO), 1030–1020 (ν_s COO) [IVa species]; 1620–1670 cm^{-1} (ν C–O), 1220–1270 cm^{-1} (ν_{as} COO), 980–1020 (ν_s COO) [IVb species].

Carbonate formation, $CO_3^=$, on the zinc oxide surface was observed by Little [24] at 1430 cm^{-1} (ν_{as}) and 1640 cm^{-1} (without attribution), whereas acetic acid adsorption produced characteristic acetate species at 2940 (ν_s CH_3), 1554 (ν_{as} OCO), 1460 (δ_{as} CH_3), 1427 (ν_s OCO) and 1311 cm^{-1} (δ_s CH_3) [24]. Mattos et al. [25], studying Pd/CeO_2 and Pt/CeO_2 catalysts, pointed to the difficulty of distinction between carbonate and acetate species from the vibration modes that occur in the region of C–O stretching. In the present work, the accurate identification of the band at 1580 cm^{-1} becomes difficult, once the adsorption of acetic acid for reference was not carried out. However, the absence of bands in the region of 1000 cm^{-1} (not shown) could be an indicative of the carboxylate species (ν_{as} $COO)^-$, whereas the vibration mode ν_s (COO^-, 1350–1420 cm^{-1}) cannot be observed due to the overlapping of other bands in this same region. It is worth noting the slight decrease of the acetate bands (1302, 1427, 1517 cm^{-1}) suggesting the transformation of these species into carboxylates.

As the sample was heated at 400 °C, a band at 1970 cm^{-1} was verified. The infrared region in the range of 2200–1700 cm^{-1} is attributed to CO adsorption on metals, and the region of 1900–1700 cm^{-1} is assigned to the adsorbed CO in the multi-coordinate or bridge form [24]. The CO adsorption on ZnO occurs in the spectra region between 2190 and 2220 cm^{-1} [24], which was not observed in this analysis (not shown). The gaseous CO forms a band around 2143 cm^{-1} [24] and presents low absorbance intensity at 400 °C (Fig. 5). In the TPD-ethanol results for $ZnHap_{troc2}$ sample CO desorption was observed at 400–700 °C, suggesting its formation from acetate species decomposition.

The carbonate formation suggests the oxidation of the adsorbed species; similar behavior was observed for catalysts using CeO_2 as a support at temperatures of 300–400 °C [20].

The admission of flowing ethanol into the DRIFTS chamber at 400 °C (Fig. 6) leads to a significant increase in the absorbance intensity of the bands at 1580, 1302, 1434, 1397 cm^{-1}, showing an immediate carbonate and acetate formation at this temperature. The ethoxide species formation also was observed in the spectra region between 3000 and 2700 cm^{-1}. The heating at 500 °C favors the decomposition of the adsorbed intermediate and gaseous CO formation is observed from the low intensity band at 2143 cm^{-1}. The band at

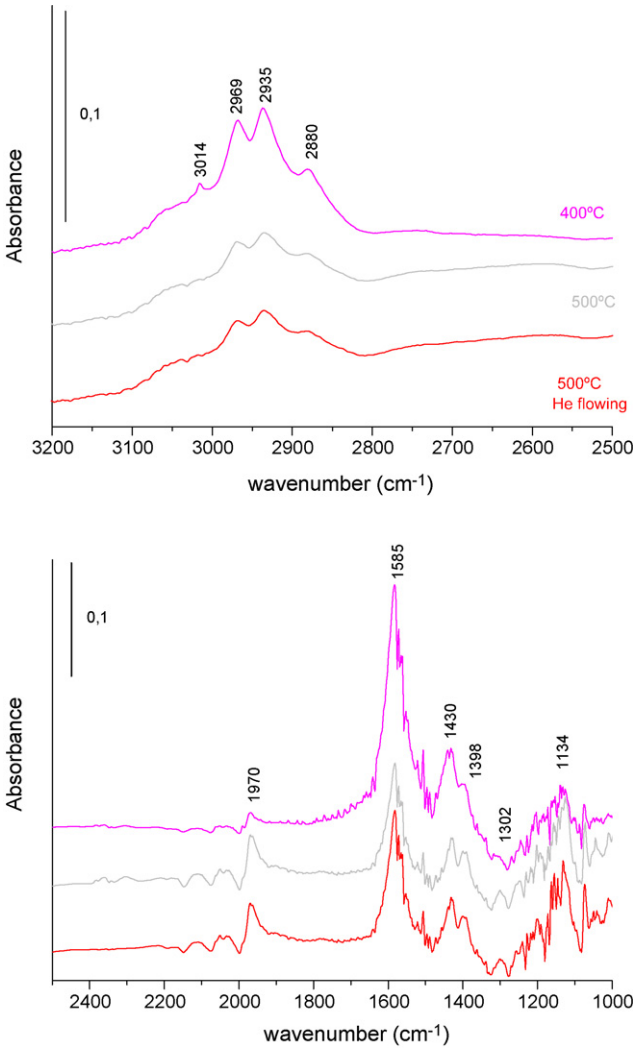

Fig. 6. DRIFT spectra after ethanol adsorption at 400 °C on $ZnHap_{troc2}$.

3014 cm^{-1} (low intensity) is associated to gaseous methane formation and suggests that the decomposition of acetate and/or carbonate leads to CH_4 and CO formation.

4. Conclusions

The Hap, synthesized by the precipitation method, was obtained with stoichiometric structure; it presented activity in the ethanol decomposition and selectivity for dehydrogenation reaction. The preparation methods used were suitable to incorporate the zinc phase and the catalysts presented significant differences in relation to the formed phase. For $ZnHap_{dep2}$ sample the ZnO was as a segregated phase and for $ZnHap_{troc2}$, Zn^{2+} was incorporated into the lattice. The deposition method revealed dependence on zinc solution concentration. The catalysts presented surface activity for the ethanol decomposition with formation of acetaldehyde and H_2. The catalysts have shown different surface reactivity and the $ZnHap_{dep2}$ presented a behavior of acidic surfaces.

For $ZnHap_{troc2}$, where Zn^{2+} substituted Ca^{2+} ions in the lattice, a high activity and selectivity was observed for the dehydrogenation reaction. DRIFTS results showed that at high temperatures acetates and carbonates were the main intermediate species.

Comparative studies of the catalysts by DRIFTS analyses and their performance in the ethanol reforming reaction are in progress to explain the differences observed in the reactivity of these surfaces.

Acknowledgments

We thank M.Sc. Carlos Andre de Castro Pérez (NUCAT/PEQ/COPPE/UFRJ) for XRD discussions and M.Sc. Marcos Anacleto (NUCAT/PEQ/COPPE/UFRJ) for TPD analyses and discussions. We also thank Conselho Nacional de Pesquisa-CNPq for the scholarship granted to Rafaella M.B. de Faria.

References

[1] M. Miyake, K. Watanabe, Y. Nagayama, H. Nagasawa, T. Suzuki, J. Chem. Soc., Faraday Trans. 86 (1990) 2303.
[2] A. Venugopal, M.S. Scurrell, Appl. Catal. 245 (2003) 137.
[3] Z. Opre, J.-D. Grunwaldt, M. Maciejewski, D. Ferri, T. Mallat, A. Baiker, J. Catal. 230 (2005) 406.
[4] S. Sugiyama, T. Shono, D. Makino, T. Moriga, H. Hayashi, J. Catal. 214 (2003) 8.
[5] K. Elkabouss, M. Kacimi, M. Ziyad, S. Ammar, F. Bozon-Verduraz, J. Catal. 226 (2004) 16.
[6] T. Hara, K. Mori, T. Mizugaki, K. Ebitani, K. Kaneda, Tetrahedron Lett. 44 (2003) 6207.
[7] S. Sugiyama, J.B. Moffat, Catal. Lett. 76 (2001) 75.
[8] H. Monma, J. Catal. 75 (1982) 200.
[9] S. Sugiyama, T. Moriga, M. Goda, H. Hayashi, J.B. Moffat, J. Chem. Soc. 92 (1996) 4305.
[10] F. Miyaji, Y. Kono, Y. Suyama, Mater. Res. Bull. 40 (2005) 209–220.
[11] N.S. Resende, M. Nele, V.M.M. Salim, Thermochim. Acta 451 (2006) 16–21.
[12] Guerra-Lopez, R. Pomes, C.O. Della Vedova, R. Vina, G. Punte, J. Raman Spectrosc. 32 (2001) 255.
[13] C.L. Kibby, W.K. Hall, J. Catal. 29 (1973) 144.
[14] N.S. Resende, F.T. Gomes, A.M. Rossi, V.M.M. Salim, In (CD_ROM): Anais 1° Encontro Brasileiro de Adsorption, Fortaleza, Brazil, 1996, p. 158.
[15] V.M.M. Salim, M.A. Silva, N.S. Resende, In (CD_ROM): Anais do 12° Congresso Brasileiro de Catálise—Novas fronteiras da Catálise, Angra dos Reis, Brazil, vol. 1, 2003, p. 306.
[16] D. Biagioni, D.V. César, N.S. Resende, V.M.M. Salim, In (CD-ROM): XIX Simposio Iberoamericano de Catálisis, Mérida, México, 2004, p. 3469.
[17] P.Y. Sheng, A. Yee, G.A. Bowmaker, H. Idriss, J. Catal. 208 (2002) 393–403.
[18] J. Llorca, N. Homs, P.R. de la Piscina, J. Catal. 227 (2004) 556–560.
[19] N. Fatsikostas, X.E. Verykios, J. Catal. 225 (2004) 439–452.
[20] L.V. Mattos, F.B. Noronha, J. Power Sources 152 (2005) 50–59.
[21] A. Yee, S.J. Morrison, H. Idriss, J. Catal. 191 (2000) 30–45.
[22] A.A. Davydov, Infrared Spectroscopy of Adsorbed Species on the Surface of Transition Metal Oxides, John Wiley & Sons, New York, 1990.
[23] A. Yee, S.J. Morrison, H. Idriss, J. Catal. 186 (1999) 275–279.
[24] L.H. Little, Infrared of Adsorbed Species, Academic Press, New York, 1966.
[25] L.V. Mattos, F.B. Noronha, J. Catal. 233 (2005) 453–463.